

Determination of Stream Function of 2D Vortex in Nonneutral Plasma and Testing Sector Probe Signals

ITO Kiyokazu*, KIWAMOTO Yasuhito¹ and SANPEI Akio

Graduate School of Human and Environmental Studies, Kyoto University, Sakyo-ku, Kyoto 606-8501, Japan

¹*Faculty of Integrated Human Studies, Kyoto University Sakyo-ku, Kyoto 606-8501, Japan*

(Received: 5 December 2000 / Accepted: 3 September 2001)

Abstract

We present a fast and sufficiently accurate procedure to construct the potential and the electric field distribution from the observed 2-D images. Such field analyses are essential for deep and extensive studies of vortex dynamics or turbulence. Using this procedure we quantitatively compare the image diagnostics with sector-probing for the first time to show that core dynamics as seen clearly with the imaging is severely obscured with the probing so that its application should be limited to simple dynamics of a small numbers of discrete distributions of particles.

Keywords:

electron plasma, sector-probe method, vortex dynamics, streamline

1. Introduction

The dynamics of a nonneutral electron plasma that is strongly magnetized and homogeneous along the magnetic field is equivalent with the two-dimensional (2D) Euler fluid. The correspondence between the density and the vorticity and that between the electric potential and the stream function ease the diagnostics and analyses of the electron vortex motion compared with those for neutral fluid vortices.

The 2D structures of the vorticity distribution are determined in terms of the luminosity distribution of electrons collected on a phosphor screen. [1-3] One disadvantage of this diagnostics, however, is that it requires dumping of the whole plasma out of the trap region. The time-varying image charge has been addressed historically with a sector probe that detects time-varying voltages induced by the vortex motion or waves without destroying the trapped plasma. [4,5]

One of the major purposes of this paper is to compare the probe signals with independently determined signals to examine the reliability of the

probe method. From the 2D density distribution we determine the potential distribution in the 2D plane. We employ Fourier-Bessel series expansion of the observed density distribution for fast numerical processing. This allows us to calculate the image charge distribution induced at the surface of the conducting sidewall.

Our study has confirmed the reliability of the sector-probe as well as the limitation of its applicability, and it is found also that the applicability can be extended by additional information derived from the luminosity distribution. This scheme of numerical processing of the luminosity distribution has also enabled us to determine stream function as seen in a coordinate system rigidly rotating around the system axis. It is quite useful for in-depth analyses of the vortex motions in a rotating frame.

2. Experimental Configuration

The electron plasma is produced by an array of small cathodes and confined in a Malmberg-trap. [1-3]

*Corresponding author's e-mail: n50116@sakura.kudpc.kyoto-u.ac.jp

With this vacuum field configuration, the axial lengths of the trapped electron columns are typically $L = 220$ mm.

The conducting cylindrical wall in the trap region is longitudinally divided into 11 rings. The 4th, 6th and 8th electrodes are azimuthally divided into 4 sectors with a uniform separation of 90 deg. We combine the three sectors at the same azimuthal locations and connect them to the virtual ground of a current amplifier through a small resistance of 300 Ω . These coupled sectors are used as an image current detector. It is well known that a resistive wall induces the diocotron instability in an electron plasma. [6-8] After careful examination and adjustment we have reached a stable circuit configuration. [3]

The transverse profile of the electron density distribution is determined from the luminosity distribution on a phosphor screen to which the trapped electrons are dumped along the magnetic field lines at each required time of measurement. [3] The conducting surface of the screen also serves as an electron collector to monitor the total number of electrons N . The luminosity distribution on the screen is detected on an array of charge-coupled device (CCD) camera. We have confirmed a good linear relationship between N and the luminosity integrated over the screen. Using the relationship we obtain the transverse distribution of the line density $N_l(x, y)$ of the plasma.

3. Analysis of the Image Data

We approximate that the chord-averaged density $n(x, y) = N_l(x, y)/L$ represents the actual density distribution of the electrons and introduce a 2D analysis in determining the potential distribution in the main part of the trapped region by neglecting effects from the ends. [3]

The potential distribution generated by the plasma is given in a 2D form $\phi(r, \theta)$ that satisfies the Poisson's equation. The contribution of the conducting wall surrounding the plasma enters as a boundary condition $\phi(R, \theta) = 0$ at the wall of a radius R .

First we Fourier-expand Poisson equation in the azimuthal angle θ to obtain a set of ordinary differential equations in the radial coordinate r . $\phi_m^{c,s}(r)$ and $n_m^{c,s}(r)$ are the m th Fourier component of the potential and the density, respectively. The density part $n_m^{c,s}(r)$ are calculated from the observed CCD images. We further expand $n_m^{c,s}(r)$ in a series of Bessel functions $J_m(z)$ to determine the associated terms of the potential that is obtained as,

$$\begin{aligned} \phi(r, \theta) = & \frac{e}{2\epsilon_0} \sum_{n=1}^{\infty} \beta_{0n}^c J_0 \left(\frac{\chi_{0n}}{R} r \right) \\ & + \frac{e}{\epsilon_0} \sum_{m=1}^{\infty} \left\{ \cos m \theta \sum_{n=1}^{\infty} \beta_{mn}^c J_m \left(\frac{\chi_{mn}}{R} r \right) \right. \\ & \left. + \sin m \theta \sum_{n=1}^{\infty} \beta_{mn}^s J_m \left(\frac{\chi_{mn}}{R} r \right) \right\}, \end{aligned} \quad (1)$$

where $J_m(\chi_{mn}) = 0$ with $n = 1, 2, 3, \dots$, and

$$\beta_{mn}^{c,s} = - \frac{2}{\{\chi_{mn} J_{m+1}(\chi_{mn})\}^2} \int_0^R dr r J_m \left(\frac{\chi_{mn}}{R} r \right) n_m^{c,s}(r). \quad (2)$$

Here the upper limit of the azimuthal mode number m_{max} and the radial mode number n_{max} are taken as $m_{max} = 100$ and $n_{max} = 100$. The calculation of the potential requires about 3 min. on a personal computer (350 MHz).

4. Testing Sector-Probe Method

Evaluating the image charge on the sector-probe surface from $\partial\phi/\partial r$ at $r = R$, we determine the image current induced on the sector-probe.

First, we observe a sector-probe signal induced by the single plasma string moving in vacuum. Figure 1(a) shows the time-varying distribution of a single electron string as observed with the CCD camera at the interval of 10 μs . The string is injected at $t = 10 \mu s$ with total electron number $N = 4.5 \times 10^7$. The string rotates clockwise along a circle with the radius of $r_0 = 8.3$ mm at the frequency of $\omega/2\pi \approx 10$ kHz.

The solid curve in Fig. 1(b) shows the current signal detected on the sector-probe. Here, we approximate that the string described by the δ -function. The image current signal can be calculated easily. [3] The image current calculated with experimental parameters of $\omega/2\pi = 9.9$ kHz, $N = 4.5 \times 10^7$, $r_0/R = 0.26$ and sector-probe length of $l = 66$ mm is plotted in a dotted curve. The dash-dotted line represents the output waveform corrected for the frequency response of the current amplifier. We can confirm a good agreement between the directly observed probe signal and the signal calculated from the CCD camera image.

Figure 2 plots the amplitudes of the sector-probe signal against N at different radii. The solid lines stand for the theoretically expected amplitude after correction of the amplifier response. These data represent the first experimental confirmation that the image diagnostics leads to results that quantitatively agree with the signals independently detected with a sector-probe.

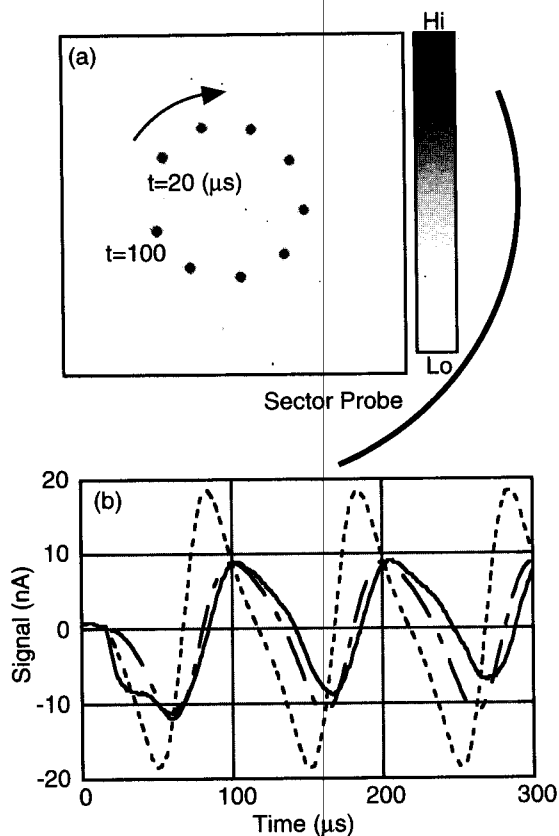


Fig. 1 (a) Motion of the single string of electrons in vacuum observed with the CCD camera. (b) Sector-probe signals induced by this motion. The solid line represents the experimentally observed signal. The dotted line shows the calculated signal and the dashed-dotted line represents the calculated signal corrected for the frequency response of the amplifier.

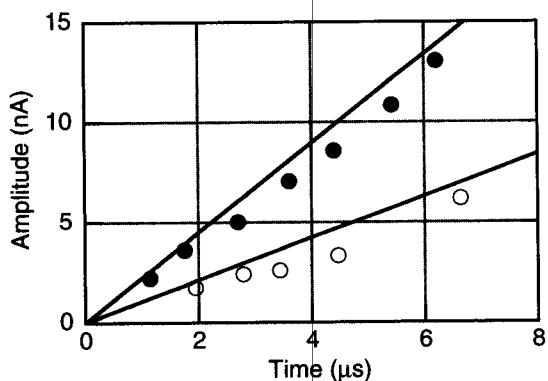


Fig. 2 Amplitudes of the sector-probe signals due to the single plasma string motion are plotted against the electron number in the string. Open circles ($r/R = 0.26$) and closed circles ($r/R = 0.12$) show the data obtained by the probe. Solid line represents the theoretical value for each case.

Next, we compare the methods for a more complicated distribution. Figures 3(a)–(d) show frames of the CCD images of the density distribution at different times. Here a plasma string with $N_L = 1.2 \times 10^7$ is injected at $t = 10 \mu\text{s}$ into the background plasma with $N_b = 1.9 \times 10^8$. It is observed that the string plasma moves toward the center of the background plasma as it rotates while creating a spiral streak behind it. [2]

The solid curve in Fig. 4 represents the experimentally observed probe signal. We try to reproduce the probe signal from the observed electron distribution that have been recorded at a step of $2 \mu\text{s}$. The calculations include the frequency response of the amplifier.

The closed circles in Fig. 4 represent the signal calculated by differentiating the image charge corresponding to each frame of the density distribution. [3] Open symbols are obtained from a calculation that takes the self-consistent drift motion of the electrons calculated from eq. (1) and continuity of the density. [3] Consideration with the contribution of the vacuum field drive with the rigid rotation at 0 (\circ), 10 (Δ), 15 (\square) kHz and with the differential drive (\times) lead to a similar waveforms supporting the consistency among these analysis. However, the image-based signals show apparent disagreement in the phase with the probe

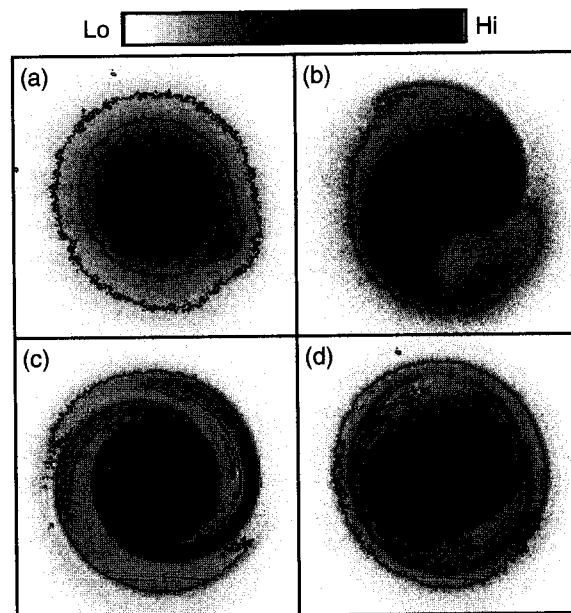


Fig. 3 2-D distribution of the electron density observed with CCD camera at different time. $t = 16$ (a), 30 (b), 40 (c) and 100 (d) μs .

signal.

The discrepancy can be reduced only by assuming the presence of electrons extending near the wall at a very low density level unable to detect with the present imaging system. [3] Here, we assume that the invisible distribution covers the section extending radially from $r/R = 0.8$ to 0.98 , azimuthally over the width of $\pi/2$ with the density level of $4.8 \times 10^{10} \text{ m}^{-3}$. The electron number of this part amounts to 1.4% of the total electron number. Another assumption is that the electrons rotate rigidly at the observed frequency of 15 kHz. The "probe signal" contributing from these electrons is plotted in the dotted line in Fig. 4. Judging from the good proximity and total consistency, we believe that this is the unique answer to the problem posed in regard to Fig. 4.

The above discussion indicates that the probe diagnostics is strongly affected by the peripheral distribution of particles if they exist though their contribution in the dynamics of the main part of the plasma is not essential.

5. Determination of Stream Function

The equipotential surfaces conform to the streamlines. In most cases, these surfaces compose a set of almost circular lines, and fine structures as observed in the density distribution are obscured in the potential profile.

The streamlines to be observed in the frame co-rotating with the point vortex are calculated as shown in Fig. 5(a)–(d) corresponding to the images in Fig. 3. [9] The density (vorticity) distribution is superposed also in each frame. We can see a set of closed lines around the point vortex and the separatrix that distinguishes the background flow in the outer region. This structure is consistent with the model discussed in Ref. 2 though the shape of the stream lines is strongly deviated inward. The separatrix expands in time as the point vortex moves inward until it reaches the center of the background vortex to form a new concentric structure of circles. It is also observed that the spiral arm extends along the stream lines

6. Conclusions

We have developed a fast procedure to numerically construct the 2D field distribution from the image data directly related to the electron density distribution. The validity and applicability of electrostatic probing diagnostics are critically examined by applying the field analysis. It also has proved to be useful to elucidate the

flow pattern around a point vortex in the rotating frame. We expect further application of this method to deep and extensive study of the vortex dynamics and statistics

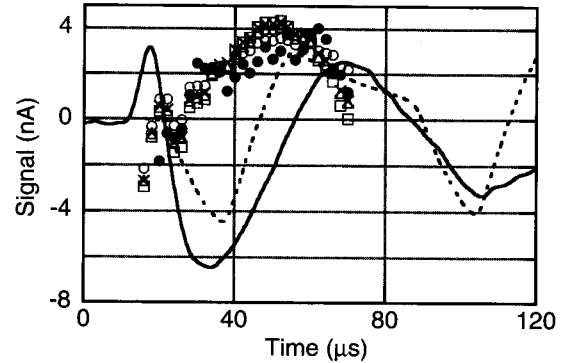


Fig. 4 Sector-probe signal detected in the case that plasma string is injected to the background plasma as shown in Figs. 3(a)–(d). The solid line represents the signal actually observed with the probe. The symbols denote the probe signal calculated from the CCD images with different methods. The dotted line shows the signal calculated with the model distribution extending to the periphery. These calculated signals are corrected for the amplifier response.

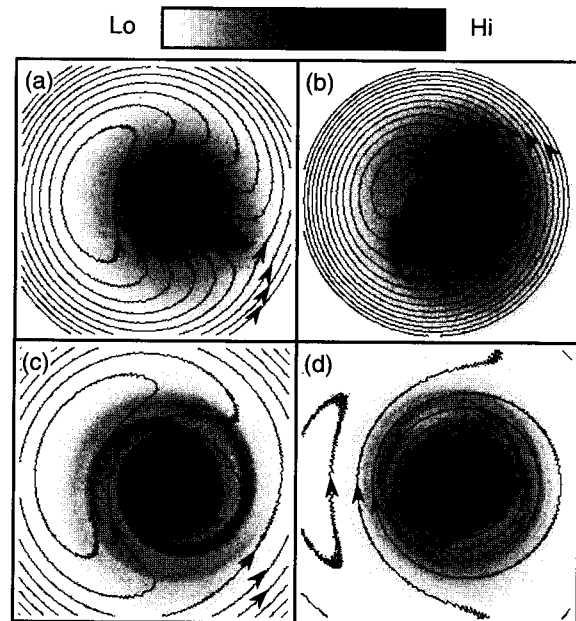


Fig. 5 Equipotential surface (streamline) and 2-D distribution of the electron density (vorticity) and at different time. $t = 16$ (a), 22 (b), 40 (c) and 100 (d) μs .

Acknowledgments

The authors thank Prof. A. Mohri for stimulating discussion. This work was supported by a Grant-in-Aid from the Ministry of Education, Science, Sports and Culture and by the collaborative research program of National Institute for Fusion Science.

References

- [1] Y. Kiwamoto, K. Ito, A. Sanpei, A. Mohri, T. Yuyama and T. Michishita, *J. Phys. Soc. Jpn. (Letter)* **68**, 3766 (1999).
- [2] Y. Kiwamoto, K. Ito, A. Sanpei and A. Mohri, *Phys. Rev. Lett.* **85**, 3173 (2000).
- [3] K. Ito, Y. Kiwamoto and A. Sanpei, *Jpn. J. Appl. Phys.* **40**, 2558 (2001).
- [4] C.A. Kapetanacos and A.W. Trivelpiece, *J. Appl. Phys.* **42**, 4841 (1971).
- [5] Roy W. Gould, *Phys. Plasmas*, **2**, 2151 (1995).
- [6] J.S. deGrassie and J.H. Malmberg, *Phys. Fluids* **23**, 63 (1980).
- [7] W.D. White, J.H. Malmberg and C.F. Driscoll, *Phys. Rev. Lett.* **49**, 1823 (1982).
- [8] B.P. Cluggish, C.F. Driscoll, K. Avinash and J.A. Helffrich, *Phys. Plasmas* **4**, 2062 (1997).
- [9] M.V. Melander *et al.*, *J. Fluid Mech.* **178**, 2062 (1997).